JOURNAL OF Materials CHEMISTRY

Long time annealing effects on the microstructures of the sol–gel-derived nanocrystalline thin films of rare earth-stabilized zirconia†

Ya-Wen Zhang, Yu Yang, Shu Jin, Chun-Sheng Liao and Chun-Hua Yan*

State Key Lab of Rare Earth Materials Chemistry and Applications & PKU-HKU Joint Lab on Rare Earth Materials and Bioinorganic Chemistry, Peking University, Beijing, 100871, China. E-mail: chyan@chem.pku.edu.cn

Received 2nd January 2001, Accepted 15th May 2001
First published as an Advance Article on the web 4th July 2001

Long time annealing effects on the microstructures of the sol–gel-derived $(ZrO_2)_{0.92}(RE_2O_3)_{0.08}$ (RE = Sc, Y, Nd, Gd, Dy, Ho, Er, Tm, Yb, Lu) and $(ZrO_2)_{0.92}(Sc_2O_3)_{0.08-x}(Y_2O_3)_x$ ($x = 0.02$–0.06) nanocrystalline thin films with the thickness of 0.6 μm on a Si(100) substrate were investigated by Auger electron spectroscopy, X-ray diffraction, scanning electron microscopy and atomic force microscopy. After annealing at 800 °C for 21 days, these films showed distinguishable microstructural variations in lattice parameter and grain size along the rare earth series, and the nanoparticle size uniformity was decreased. Among the rare earth-stabilized zirconia thin films, $(ZrO_2)_{0.92}(Y_2O_3)_{0.08}$ and $(ZrO_2)_{0.92}(Nd_2O_3)_{0.08}$ films displayed the best microstructural thermal stability with the least lattice variation and grain growth on annealing. On the other hand, the as-deposited $(ZrO_2)_{0.92}(Sc_2O_3)_{0.08-x}(Y_2O_3)_x$ ($x = 0.02$–0.06) films exhibited better microstructural thermal stability than the $(ZrO_2)_{0.92}(Sc_2O_3)_{0.08}$ films.

Introduction

Fabrication methodology and electrical properties of ceramic electrolyte thin films employed in the electrochemical devices such as oxygen sensors and fuel cells have drawn intensive interest for several years.[1–3] As the heart of these devices, the thin films are required to exhibit high electrical conductivity, high mechanical strength, heat resistance, chemical durability and good microstructural thermal stability at the operating temperatures of 800–1000 °C. Normally, the commercial devices should have an operating life of at least 3–5 years.[4] In order to prolong the device life, deterioration of electrical properties of the electrolyte films due to annealing-induced microstructural variation and grain growth needs be avoided as much as possible during long time operation.

As is well known, annealing conditions (temperature, time, method and atmosphere) play a significant role in determining the microstructures and properties of the ceramic electrolytes.[4,5] Previously, some authors reported the electrical aging behavior of yttria- or scandia-stabilized zirconia (as the candidate electrolyte employed in the electrochemical devices) bulk materials upon annealing.[4–10] In the case of thin films, much attention has been paid to the development of fabrication techniques and the annealing temperature effects upon the phase evolution and grain size of the electrolyte during the synthesis; however, investigations into annealing time effects (especially long time annealing) were inadequate.[11–13] Therefore, it is of considerable necessity to investigate the effects of annealing upon electrolyte films. Successful investigations are expected to benefit the efforts of improving the microstructural thermal stability of electrolyte films *via* microstructural tailoring with a rational fabrication technique, and finally extending the operating life of the devices.

Though the features of various fabrication methods have been gradually understood, the relationship between microstructure and properties of the electrolytes in the nanosize region has not been clearly established.[3] More recently, we prepared a series of rare earth-stabilized zirconia thin films (dense, crack-free and homogeneous) on a single crystal Si substrate using a simple sol–gel spin coating method,[14] and observed an enhanced ionic conduction in $(ZrO_2)_{0.92}(RE_2O_3)_{0.08}$ (RE = Sc, Y) films which was attributed to a decrease in grain boundary resistance related to interfacial effects.[15] In this study, long time annealing effects on this series of films has become our interest. On the other hand, the relationship between the annealing effects and the size of the doped rare earth ions is attractive as well. In the past, some researchers experimentally and/or theoretically investigated the size effects of some rare earths on the lattice parameters of zirconia-based solid electrolytes,[16,17] but the annealing effects on the microstructures were rarely mentioned.

The objectives of this research are to investigate the long time annealing effects on the microstructure of the sol–gel-derived $(ZrO_2)_{0.92}(RE_2O_3)_{0.08}$ (RE = Sc, Y, Nd, Gd, Dy, Ho, Er, Tm, Yb, Lu) and $(ZrO_2)_{0.92}(Sc_2O_3)_{0.08-x}(Y_2O_3)_x$ ($x = 0.02$–0.06) thin films, and to understand the relationship between the annealing effects and rare earth ion radius. Here, we present the results of annealing effects upon the film–substrate interaction, variations of lattice parameter and grain size, and morphology explored using Auger electron spectroscopy (AES), X-ray diffraction (XRD), scanning electron microscopy (SEM) and atomic force microscopy (AFM).

Experimental

Synthesis

The coating solution used had an optimized composition which contained metal ion and poly(ethylene glycol) concentrations of 0.10 M and 40 mg ml^{-1}, respectively.[14] It was prepared by dissolving the required amount of rare earth nitrate (99.95–99.99%), zirconium oxochloride (AR grade) (at the molar ratio of RE : Zr = 0.16 : 0.92), and poly(ethylene glycol) (PEG, C.P., molecular weight *ca.* 20 000) in the appropriate amount of ethanol/water solvents at the volume ratio of 8 : 1. To avoid

†Electronic supplementary information (ESI) available: XRD patterns of $(ZrO_2)_{0.92}(RE_2O_3)_{0.08}$ (RE = Sc, Y, Nd, Gd, Ho, Tm, Lu) and $(ZrO_2)_{0.92}(Sc_2O_3)_{0.04}(Y_2O_3)_{0.04}$ thin films before and after long time annealing. See http://www.rsc.org/suppdata/jm/b1/b100031o/

precipitation of metal hydroxide, drops of concentrated nitric acid were added in to the coating solution to maintain a pH value below 1.5. Before filtration, the coating solution was stirred for 2 h at room temperature.

With the as-prepared coating solution, thin films were deposited on clean, monocrystalline silicon (100) wafers through repeating the cycle of spin-coating (at a speed of 4000 rpm for 8 s), drying (at 110 °C for 20 min) and gel-firing (at 400 °C for 30 min). The sol–gel-derived thin films were annealed at the temperature of 950 °C for 2 h in an oxygen-flowing atmosphere, and the film thickness was determined by SEM to be *ca.* 0.6 μm. The effects of annealing the films at 800 °C for 21 days were then investigated.

Instruments

The as-given molar ratio of metal ions in the coating solution was standardized using an inductively coupled plasma atomic emission spectrometer (Leeman Lab. Inc.). The determined molar ratio of RE : Zr was in the range 0.176 : 0.912–0.144 : 0.923, which is in agreement with the theoretical composition of RE : Zr = 0.16 : 0.92. The surface and bulk composition of the films was studied using an Auger electron spectroscope (PHI-610) using a primary electron-beam energy of 3.0 keV and an emission current of 25 mA. The depth profile was measured using argon ion sputtering at the speed of 25 nm min^{-1}. The phase state of nanocrystals was identified using an X-ray powder diffractometer (Rigaku D/max-2000) using Cu-Kα radiation ($\lambda = 1.5408$ Å) at a scanning rate of 4° min^{-1} over the 2θ range 25–65°. The thin film thickness was determined by SEM (AMARY 1910FE), and the surface structures were probed by both SEM and AFM (Auto Probe CP, PSI).

Data treatment

Using the software 'LAPOD' for least-squares refinement of cell dimensions from powder data by Cohen's Method,[18,19] the lattice parameters have been calculated. The average grain size d_g was estimated according to the Scherrer equation,[20]

$$d_g = 0.90\lambda/\beta\cos\theta$$

where θ is the diffraction angle of the (111) peak, and β is the full-width-at-half-maximum (FWHM) of the (111) peak (in radians), which is calibrated from high purity silicon.

Results and discussion

Film–substrate interaction

The film–substrate interaction was examined first of all, so as to ensure that the films had a good composition and high purity within a certain depth range upon annealing. Typically, the surface and in-depth compositions of the $(ZrO_2)_{0.92}(Sc_2O_3)_{0.08}$ thin films were characterized by AES. On the film surface, only Zr, Sc and O atoms were detected with some carbon atoms, which were ascribed to the environmental contaminants which could be removed by argon ion-sputtering for a few minutes.[14] Prior to long time annealing, the films appear to have a three-layer structure – electrolyte (500 nm)/interdiffusion layer (< 100 nm)/Si substrate – [see Fig. 1(a)], in which the inter-diffusion layer is formed by the chemical reaction between the substrate and the film with formation of chemical species such as SiO_2 and $ZrSiO_4$.[21,22] The films are fairly pure with good composition homogeneity within the depth range 75–500 nm and with the atomic ratio of Sc : Zr : O = 1 : 3.5 : 5.7, which deviates a little from the theoretical ratio of 1 : 5.75 : 13.

After long time annealing, the films display a nearly constant composition within the depth range 200–1000 nm with the atomic ratio Sc : Zr : O = 1 : 4.8 : 8.7 and a four-layer structure [electrolyte (1000 nm)/interdiffusion layer (< 100 nm)/SiO_2 (400 nm)/Si substrate], as shown in Fig. 1(b). Upon annealing, the SiO_2 layer was formed due to the slow oxidation by the migrated oxygen from the electrolyte layer, as was consistently observed during the synthesis of ZrO_2 films on Si(100).[22] Above 400 °C, annealing of the ZrO_2/Si stack in O_2 increased the interfacial SiO_2 layer.

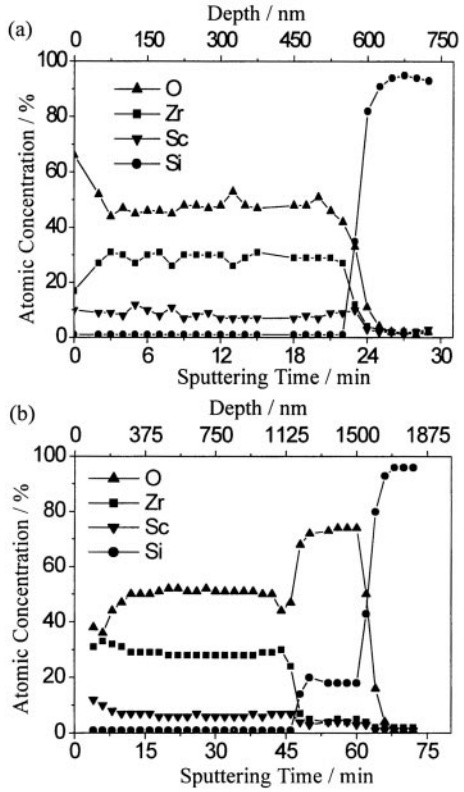

Fig. 1 In-depth AES compositional profile of the $(ZrO_2)_{0.92}(Sc_2O_3)_{0.08}$ thin films before (a) and after (b) long time annealing.

As described above, upon annealing, the thickness of the interdiffusion layer was much thinner than that of the electrolyte layer; this confirms that a well defined film–substrate interface was formed and indicates that no significant interdiffusion occurred.[23]

Lattice parameter and grain size variations

During annealing, $(ZrO_2)_{0.92}(RE_2O_3)_{0.08}$ (RE = Y, Nd, Gd, Dy, Ho, Er, Tm, Yb, Lu) and $(ZrO_2)_{0.92}(Sc_2O_3)_{0.08-x}(Y_2O_3)_x$ films appeared in a pure cubic phase. In the case of $(ZrO_2)_{0.92}(Sc_2O_3)_{0.08}$ films, 19% cubic nanocrystals were transformed to the monoclinic phase after long time annealing. The percentage of the monoclinic phase was calculated from the relative peak area of the monoclinic (m) peaks $(1\ 1\ \bar{1})_m$ + $(1\ 1\ 1)_m$ and the monoclinic plus cubic (c) peaks $(1\ 1\ \bar{1})_m$ + $(1\ 1\ 1)_m$ + $(1\ 1\ 1)_c$. Comparison of the XRD patterns of the $(ZrO_2)_{0.92}(RE_2O_3)_{0.08}$ (RE = Sc Y, Nd, Gd, Ho, Tm, Lu) and $(ZrO_2)_{0.92}(Sc_2O_3)_{0.04}(Y_2O_3)_{0.04}$ films before and after long time annealing (see ESI†) reveals broadening of the diffraction peaks indicating nanocrystal formation in these films.

Fig. 2 shows the plot of lattice parameter a as a function of the Shannon radius[24] of the trivalent rare earth ions (presumably eight-coordinated) $r(RE^{3+})$ before and after long time annealing, for which the dashed line represents the lattice parameter a_0 of pure cubic ZrO_2 (therein, $a_0 = 5.085$ Å). Prior to long time annealing, the lattice parameter variation tendency of $(ZrO_2)_{0.92}(RE_2O_3)_{0.08}$ nanocrystals was confused because the phase state of the films still had not acquired equilibrium after annealing at 950 °C for 2 h. After annealing at 800 °C for 21 d, the lattice parameter value varied according to

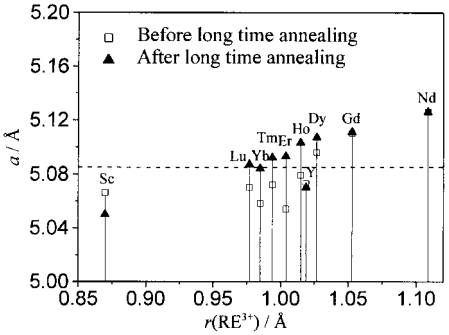

Fig. 2 Lattice parameter a of $(ZrO_2)_{0.92}(RE_2O_3)_{0.08}$ (RE = Sc, Y, Nd, Gd, Dy, Ho, Er, Tm, Yb, Lu) thin films as a function of rare earth ion radius $r(RE^{3+})$ before and after long time annealing.

the order of $a(Sc) < a(Y) < a(Lu) \approx a(Yb) < a(Tm) \approx a(Er) < a(Ho) < a(Dy) < a(Gd) < a(Nd)$, which is the result of redistribution of cations and/or anions during annealing. This order basically agrees with the fact that the lattice parameter tends to increase with increasing the radius of the rare earth ion,[16,17] except for yttria-doped nanocrystals. The as-calculated lattice parameter a of the Sc-, Y-, Gd- or Yb-doped nanocrystals is a little shorter compared with that of the respective microcrystalline material.[17] It is also noted that the lattice parameter value of Sc- or Y-doped nanocrystals is shorter than that of pure cubic ZrO_2 crystals; whereas, that of Nd-, Gd-, Dy- or Yb-doped nanocrystals is longer. In the case of Lu- or Yb-doped nanocrystals, the lattice parameter value is very close to 5.085 Å. After a long annealing time, a slight shrinkage occurs with the Sc-doped nanocrystal lattice, whereas with Dy-, Ho-, Er-, Tm-, Yb- or Lu-doped nanocrystal lattices a little expansion occurs. Interestingly, the lattices of Y-, Nd- or Gd-doped nanocrystals show little variation on long time annealing.

Fig. 3 shows the plot of average grain size d_g as a function of $r(RE^{3+})$ before and after long time annealing. It is observed that all the rare earth-doped nanocrystals grow on long time annealing. Sc-doped nanocrystals display the highest growth tendency, whereas Y- or Nd-doped nanocrystals exhibit the lowest.

The grain size variation percentage α_1 and lattice parameter variation percentage α_2 can be defined by $\alpha_1 = 100(d_g' - d_g)/d_g$ and $\alpha_2 = 100(a' - a)/a$, respectively. Here, d_g and d_g' are the average grain size before and after long time annealing, respectively, and a and a' are the lattice parameter before and after long time annealing, respectively. If α_1 is plotted against α_2, as shown in Fig. 4 (the dashed line indicates that the lattice parameter variation percentage of pure cubic ZrO_2 is zero), it is seen that the nanograins grow prominently with drastic expansion or shrinkage of the nanocrystal lattice in the case of Dy, Ho, Er, Tm, Yb, Lu or Sc-doped nanocrystals, whereas Y- or Nd-doped nanocrystals grow little with the least lattice

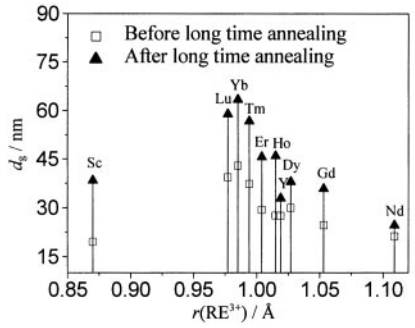

Fig. 3 Average grain size d_g of $(ZrO_2)_{0.92}(RE_2O_3)_{0.08}$ (RE = Sc, Y, Nd, Gd, Dy, Ho, Er, Tm, Yb, Lu) thin films as a function of rare earth ion radius $r(RE^{3+})$ before and after long time annealing.

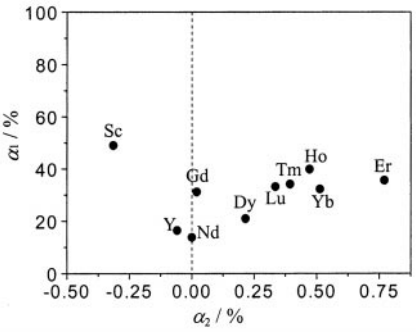

Fig. 4 Lattice variation percentage α_1 of $(ZrO_2)_{0.92}(RE_2O_3)_{0.08}$ (RE = Sc, Y, Nd, Gd, Dy, Ho, Er, Tm, Yb, Lu) thin films as a function of grain size variation percentage α_2 after long time annealing.

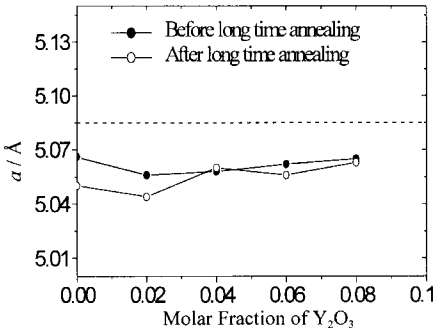

Fig. 5 Lattice parameter a of $(ZrO_2)_{0.92}(Sc_2O_3)_{0.08-x}(Y_2O_3)_x$ thin films as a function of Y_2O_3 molar fraction before and after long time annealing.

variation. This strongly suggests that drastic lattice variation could more or less induce and accelerate the nanocrystal growth during long time annealing. Among the rare earth-stabilized zirconia films, the best microstructural thermal stability can be obtained for Y- or Nd-doped nanocrystals.

Upon annealing, the observation of cubic phase decomposition and drastic microstructural variation in $(ZrO_2)_{0.92}$-$(Sc_2O_3)_{0.08}$ films indicates that the Sc-doped nanocrystals are metastable in nature. Therefore, the microstructural thermal stability of $(ZrO_2)_{0.92}(Sc_2O_3)_{0.08}$ films remains a problem and needs improving. Referring to the foregoing results, the improvement may be realized by substituting yttria for scandia. Fig. 5 and Fig. 6 depict the plot of lattice parameter a and the average grain size d_g against the molar fraction of yttria in $(ZrO_2)_{0.92}(Sc_2O_3)_{0.08-x}(Y_2O_3)_x$ films, respectively. Strikingly, with an increase in x from 0.02 to 0.06, the lattice variation and grain growth of the nanocrystals with the given composition tend to be restrained on long time annealing. As already

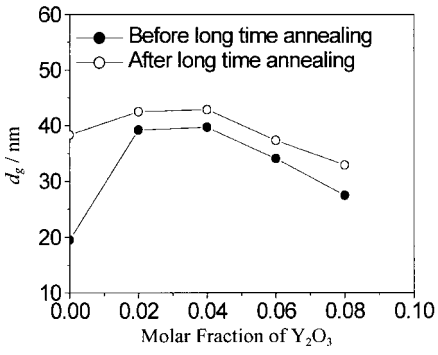

Fig. 6 Average grain size d_g of $(ZrO_2)_{0.92}(Sc_2O_3)_{0.08-x}(Y_2O_3)_x$ thin films as a function of Y_2O_3 molar fraction before and after long time annealing.

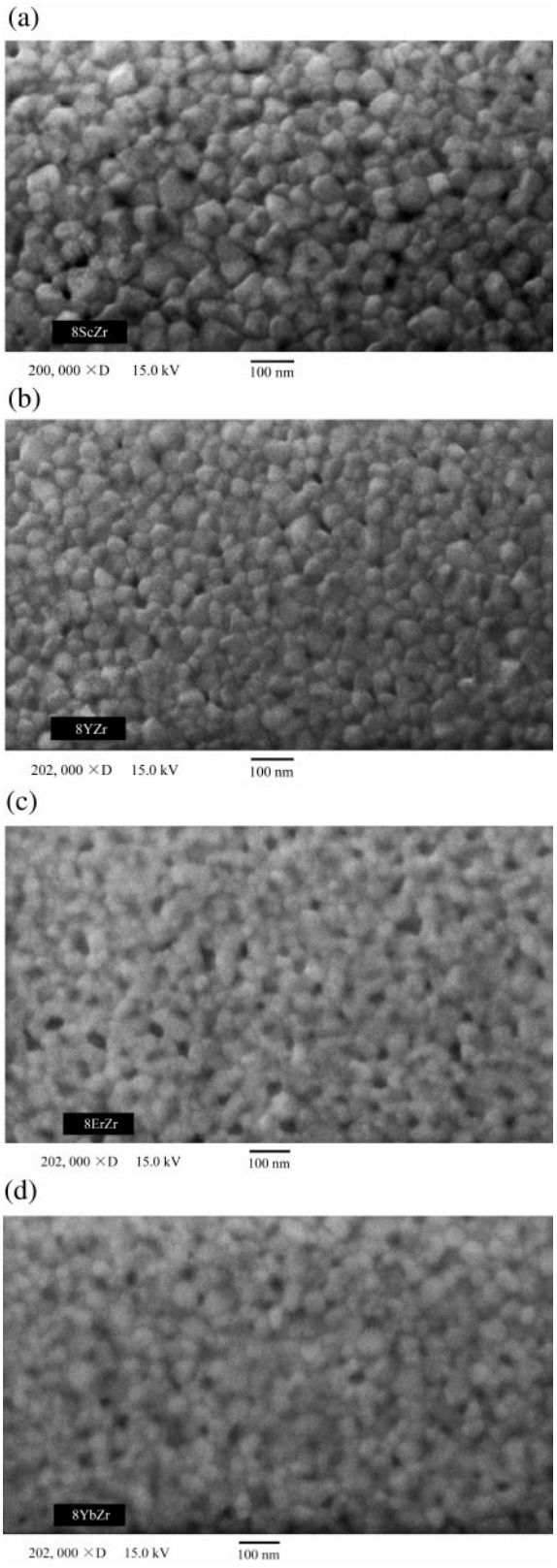

Fig. 7 Surface SEM micrographs of $(ZrO_2)_{0.92}(Sc_2O_3)_{0.08}$ (a), $(ZrO_2)_{0.92}(Y_2O_3)_{0.08}$ (b), $(ZrO_2)_{0.92}(Er_2O_3)_{0.08}$ (c) and $(ZrO_2)_{0.92}(Yb_2O_3)_{0.08}$ (d) thin films before long time annealing.

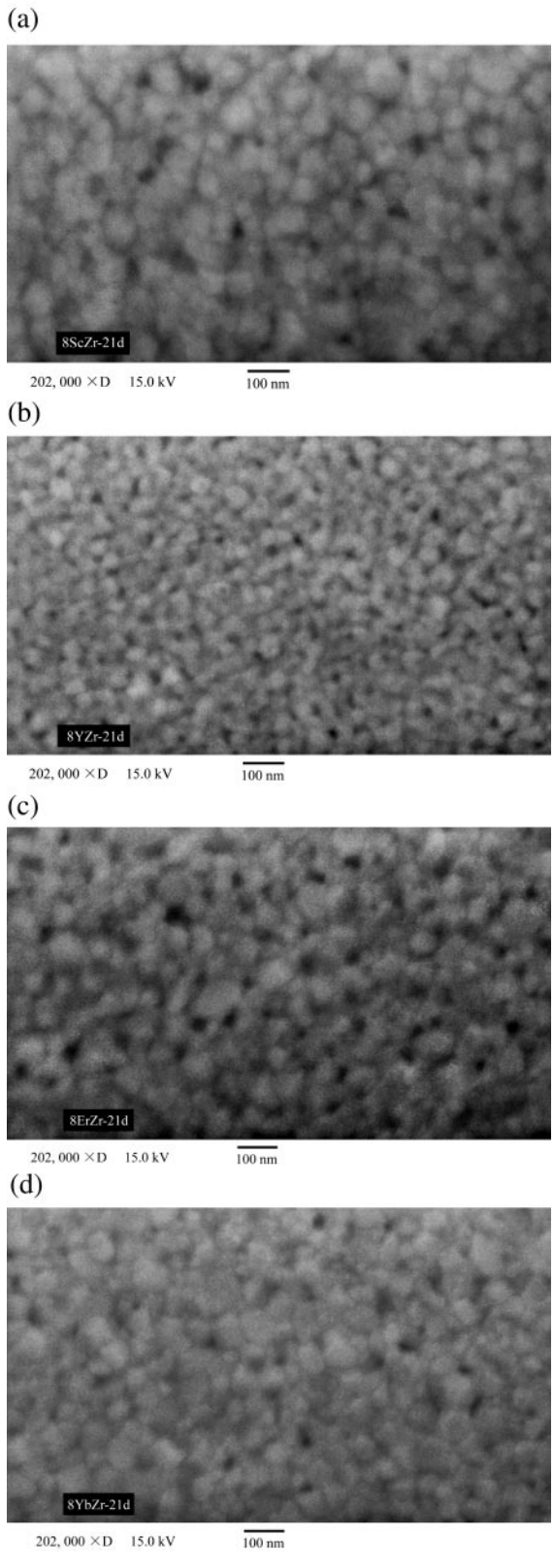

Fig. 8 Surface SEM micrographs of $(ZrO_2)_{0.92}(Sc_2O_3)_{0.08}$ (a), $(ZrO_2)_{0.92}(Y_2O_3)_{0.08}$ (b), $(ZrO_2)_{0.92}(Er_2O_3)_{0.08}$ (c) and $(ZrO_2)_{0.92}(Yb_2O_3)_{0.08}$ (d) thin films after long time annealing.

illustrated above, the cubic $(ZrO_2)_{0.92}(Sc_2O_3)_{0.08-x}(Y_2O_3)_x$ nanocrystals showed no phasic decomposition. Previously, a similar effect was reported for polycrystalline $(ZrO_2)_{0.92}$-$(Sc_2O_3)_{0.08}$ by Badwal and coworkers.[25,26] They observed that $(ZrO_2)_{0.92}(Sc_2O_3)_{0.08}$ in the t′-phase (tetragonal symmetry) slowly decomposed with time into a cubic phase matrix with tetragonal precipitates in the 700–1000 °C temperature range.[25] The phasic decomposition could result in conductivity degradation, which could be reduced by successively replacing scandia with yttria in polycrystalline $(ZrO_2)_{0.92}(Sc_2O_3)_{0.08}$.[26]

As can also be seen from Fig. 5, unlike the case of the corresponding microcrystalline materials,[27] the lattice parameter a of $(ZrO_2)_{0.92}(Sc_2O_3)_{0.08-x}(Y_2O_3)_x$ thin films does not exhibit an obvious linear increase as x is increased from zero to 0.06. On the other hand, upon increasing x from 0.04 to 0.08,

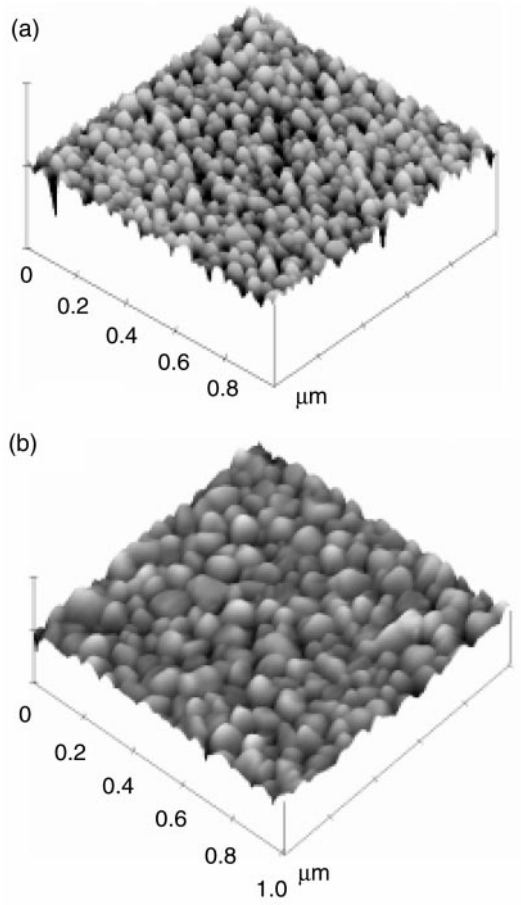

Fig. 9 Three-dimensional AFM micrographs of $(ZrO_2)_{0.92}(Y_2O_3)_{0.08}$ thin films before (a) and after (b) long time annealing.

the average grain size of the films decreases before long time annealing, because the presence of the yttria dopant inhibits atomic mobility during film growth. A similar variation was observed in nanocrystalline yttria-stabilized zirconia thin films.[28]

Morphological variation

SEM and AFM micrographs obtained in this research reveal that long time annealing has substantial effects upon the morphology of the as-deposited nanocrystalline thin films. Fig. 7 and Fig. 8 representatively exhibit the surface micrographs of Sc-, Y-, Er- and Yb-doped films before and after long time annealing, respectively. When Fig. 8 is compared with Fig. 7, it can be seen that the nanoparticles grow larger after long time annealing. Upon annealing, Y- and Sc-doped films displayed the least and greatest grain growth tendency, respectively. This result agrees well with that obtained by XRD line broadening analysis. AFM micrographs show that long time annealing could decrease the size uniformity of the nanoparticles. As an example, the three dimensional AFM micrographs of $(ZrO_2)_{0.92}(Y_2O_3)_{0.08}$ films before and after long time annealing are given in Fig. 9, from which it is noticed that the nanoparticles grow from *ca.* 55 to *ca.* 80 nm after long time annealing.

Conclusions

Long time annealing effects on the sol–gel-derived rare earth-stabilized zirconia nanocrystalline thin films have been explored in this paper. Upon annealing, a SiO_2 layer was formed on the Si substrate as the substrate was gradually oxidized by the oxygen which migrated from the electrolyte layer. The experimental results also show that long time annealing can not only induce lattice variation and grain growth with these films, but can also lower the nanoparticle size uniformity. These effects might be regarded as a sign of the aging of the ceramic electrolytes. Among the rare earth-doped zirconia films, $(ZrO_2)_{0.92}(Y_2O_3)_{0.08}$ and $(ZrO_2)_{0.92}(Nd_2O_3)_{0.08}$ films display the best microstructural thermal stability upon annealing. By substituting yttria for scandia, the microstructural thermal stability of $(ZrO_2)_{0.92}(Sc_2O_3)_{0.08}$ films can be improved.

Acknowledgements

Grants-in-aid from NSFC (Nos. 29525101, 29701001 and 29832010), the State Key Project on Fundamental Research of MOST (G1998061300), the Training Project for Doctoral Student of MOE, and Founder Group Corporation Foundation of Peking University are gratefully acknowledged.

References

1 J. Will, A. Mitterdorfer, C. Kleinlogel, D. Perednis and L. J. Gauckler, *Solid State Ionics*, 2000, **131**, 79.
2 B. Zhu, *Solid State Ionics*, 1999, **119**, 305.
3 H. L. Tuller, *Solid State Ionics*, 2000, **131**, 143.
4 J. Drennan, *J. Mater. Synth. Process.*, 1998, **6**, 181.
5 S. P. S. Badwal, *Solid State Ionics*, 1992, **52**, 23.
6 K. Nomura, Y. Mizutani, M. Kawai, Y. Nakamura and O. Yamamoto, *Solid State Ionics*, 2000, **132**, 235.
7 S. P. S. Badwal, F. T. Ciacchi and D. Milosevic, *Solid State Ionics*, 2000, **136–137**, 91.
8 S. P. S. Badwal, F. T. Ciacchi, S. Rajendran and J. Drennan, *Solid State Ionics*, 1998, **109**, 167.
9 O. Yamamoto, Y. Arachi, Y. Takeda, N. Imanishi, Y. Mizutani, M. Kawai and Y. Nakamura, *Solid State Ionics*, 1995, **79**, 137.
10 S. P. S. Badwal, *J. Mater. Sci.*, 1987, **22**, 4125.
11 C. R. Xia, H. Q. Cao, H. Wang, P. H. Yang, G. Y. Meng and D. K. Peng, *J. Membr. Sci.*, 1999, **162**, 181.
12 J. Kim and Y. S. Lin, *J. Membr. Sci.*, 1998, **139**, 75.
13 J. S. Lee, T. Matsubara, T. Sei and T. Tsuchiya, *J. Mater. Sci.*, 1997, **32**, 5249.
14 Y. W. Zhang, Y. Yang, S. Jin, S. J. Tian, G. B. Li, J. T. Jia, C. S. Liao and C. H. Yan, *Chem. Mater.*, 2001, **13**, 372.
15 Y. W. Zhang, S. Jin, Y. Yang, G. B. Li, S. J. Tian, J. T. Jia, C. S. Liao and C. H. Yan, *Appl. Phys. Lett.*, 2000, **77**, 3409.
16 M. O. Zacate, L. Minervini, D. J. Bradfield, R. W. Grimes and K. E. Sickafus, *Solid State Ionics*, 2000, **128**, 243.
17 D. W. Strickler and W. G. Carlson, *J. Am. Ceram. Soc.*, 1965, **48**, 286.
18 J. I. Langford, *J. Appl. Crystallogr.*, 1971, **4**, 259.
19 J. I. Langford, *J. Appl. Crystallogr.*, 1973, **6**, 190.
20 A. Guinier, in *Theorie et Technique de la Radiocristallographie*, Dunod, Paris, 3rd edn., 1964, p. 482.
21 A. Galtayries, M. Crucifix, G. Blanchard, G. Terwagne and R. Sporken, *Appl. Surf. Sci.*, 1999, **142**, 159.
22 Y.-M. Sun, J. Lozano, H. Ho, H. J. Park, S. Veldman and J. M. White, *Appl. Surf. Sci.*, 2000, **161**, 115.
23 C. C. Chen, M. M. Nasrallah and H. U. Anderson, *J. Electrochem. Soc.*, 1993, **140**, 3555.
24 R. D. Shannon, *Acta Crystallogr., Sect. A*, 1976, **32**, 751.
25 S. P. S. Badwal and J. Drennan, *Solid State Ionics*, 1992, **53–56**, 769.
26 F. T. Ciacchi and S. P. S. Badwal, *J. Eur. Ceram. Soc.*, 1991, **7**, 197.
27 H. Kaneko, F. Jin, H. Taimatsu and H. Kusakabe, *J. Am. Ceram. Soc.*, 1993, **76**, 793.
28 M. Boulouz, A. Boulouz, A. Giani and A. Boyer, *Thin Solid Films*, 1998, **323**, 85.